MULTI-SCALE IMAGING OF RESPIRATORY BACTERIAL INFECTION USING

FIBER MICROENDOSCOPY AND WHOLE-ANIMAL IMAGING

A Thesis

by

JOEL NATHAN BIXLER

Submitted to the Office of Graduate and Professional Studies of
Texas A&M University
in partial fulfillment of the requirements for the degree of

MASTER OF SCIENCE

Chair of Committee,   Kristen C. Maitland
Committee Members,   Vladislav V. Yakovlev
                          Jeffrey D. Cirillo
Head of Department,   Gerard L. Cote

December 2014

Major Subject: Biomedical Engineering

ABSTRACT

We have integrated a fluorescence microendoscope into a whole-animal optical imaging system, allowing for simultaneous microscopic and macroscopic imaging of tdTomato expressing BCG in vivo. A 535 nm LED was collimated and launched into a 10,000 element fiber bundle with an outer diameter of 0.66 mm. The fiber bundle can be inserted through an intra-tracheal catheter into the lung of a mouse. Fluorescence emission can either be (1) collected by the bundle and imaged onto the surface of a CCD camera for localized detection or (2) the fluorescence can be imaged by the whole animal imaging system providing macroscopic information. Results from internal localized excitation and external whole body detection indicate the potential for imaging bacterial infections down to 100 colony forming units. This novel imaging technique has the potential to allow for functional studies, enhancing the ability to assess new therapeutic agents.

DEDICATION

To my parents, Nathan and Mary

ACKNOWLEDGEMENTS

I would like to thank my committee chair, Dr. Kristen Maitland, and my committee members, Dr. Jeffrey Cirillo and Dr. Vladislav Yalovlev, for their guidance and support during these experiments. I would also like to extend my thanks to Dr. Ying Kong for his assistance in the animal imaging study. Without their support, none of this work would be possible.

I would also like to thanks my parents for their continual support during my tenure at Texas A&M, as well as my friends and colleagues within the department that encouraged me along the way.

TABLE OF CONTENTS

LIST OF FIGURES

1   INTRODUCTION

Whole-animal fluorescence imaging has recently found widespread use in the biological sciences. Fluorescence based techniques have long been used to study biological specimens, both fixed and alive, as they allow highly selective and specific detection of molecules even at low concentrations (1). With advances in both light sources and detectors, whole-animal fluorescence imaging has found widespread use in preclinical studies ranging from disease progression to response to therapy to the development of novel probes (2). While traditional fluorescence microscopy requires the sacrifice of multiple animals at discrete time points, whole-animal imaging allows researchers to study disease progression or the efficacy of a therapeutic agent more precisely than prior imaging techniques (3). Whole-animal imaging has been used to study a wide range of organ systems. These include neurological conditions, such as brain cancer (4) and neurological degenerate disease (5), cardiovascular conditions such as atherosclerosis (6) and myocardial infarction (6, 7), as well as the study of respiratory infections such as tuberculosis (8).

Recent advances in fiber optic technology have allowed for the development of novel optical imaging systems including fiber based microendoscopes (9). These systems typically image using either proximal or distal scanning of a fiber optic. Proximal scanning at the system side of the fiber is typically achieved through a coherent image guide, such as a fiber bundle, that relays a scanned patter to a tissue sample (10). This has the advantage that the size of the scanning mirrors are not constrained, allowing for the use of

more readily available commercial scanning systems. These types of systems are limited in resolution by the fiber bundle, where the core size and number of fibers limits the resolution and number of pixels respectively. For efficient collecting, miniaturized objective lenses, or gradient refractive lens (GRIN) lens systems are often employed (11, 12). Conversely, if no lens system is employed, efficient collection only occurs when the probe is in contact with the tissue sample being examined.

This thesis highlights the incorporation of a custom built fiber microendoscope into a commercial Caliper *in-vivo* Imaging system (IVIS) for multi-scale *in vivo* imaging of respiratory infections in an animal model. By combining these two systems, significant enhancement is seen in the effective detection sensitivity. This combination of imaging systems has the potential to aid in the study of a variety of infectious agents, as well as assist in the assessment of drug based therapies.

2   BACKGROUND AND MOTIVATION

2.1 Background

Imaging technologies could reduce the impact of respiratory diseases on health by drastically improving the specificity of detection as compared with traditional diagnostic methods. Diagnosis of respiratory diseases normally occurs by observation of clinical symptoms and is confirmed by chest X-ray. These methods cannot diagnose the specific agent, so subsequent sputum collection is performed for culture, biochemical analysis, differential stains, and agent identification. In many cases, such as with children, the collection of sputum cannot always be obtained. Because of this, imaging technologies that allow for the specific identification of the infectious agent involved would greatly improve diagnosis. In addition, such technology could allow for the real time analysis of therapeutic efficacy. Although optical imaging probes are not always easily translatable to a clinical setting, they are inexpensive and provide a good means for animal studies. In addition, modified substrates have potential for radiological imaging (PET/SPECT) or can be applied clinically using microendoscopy. There are currently no other methods that allow for the analysis of pathogens in real time, localization of infected tissues, and immediate feedback on interventions. Thus, the development of this new technology can greatly impact diagnosis, treatment, and prevention strategies that are important for many areas of medicine.

Despite this, for many applications, increased detection sensitivity could greatly enhance the ability to study pathogenesis in more physiological relevant conditions. For

instance, detection of *Mycobacterium tuberculosis* (Mtb) has been demonstrated *in vivo* for subcutaneous infections of 10^5 colony forming units (CFU) (13). Significant enhancement of detection sensitivity could greatly enhance the ability to study the progression of respiratory infection from the onset of infection.

Excitation intensities fall off exponentially as light propagates through tissue, where this loss typically plays a dominate roll in detection sensitivity in whole-animal fluorescence imaging. Absorption of excitation radiation decays based on the Beer-Lambert law given:

$$T = \frac{I}{I_0} = e^{\sigma l N}$$

where T is the transmittance, I_0 and I are the intensity of the incident and transmitted radiation respectively, σ is the attenuation cross section, l is the pathlenght, and N is the concentration of any absorber. The absorption cross section of biological samples typically decreases as a function of wavelength throughout the visible spectrum. This allows for more radiation to safely be delivered to a tissue sample at longer wavelengths without causing thermal damage (14). Despite this, it is difficult to find a fluorophore with high quantum yeild that is excited in the near-infrared (NIR), and thus shorter wavelength radiation is needed for efficient excitation.

Delivering the excitation light directly to the target area inside of animal that is placed in a whole-animal imaging system could greatly enhance the ability to measure weak fluorescence signal from deep within the animal model. The resulting fluorescent emission is based upon the quantum yield (Φ) of the fluorophore selected, where

4

$$\Phi = \frac{number\ of\ photons\ emitted}{number\ of\ photons\ absorbed}$$

By delivering more excitation radiation to the location of the fluorophore, more signal can be generated. Since the emission is of a longer wavelength, this radiation will be more weakly attenuated by the tissue, resulting in lower detection limits while still allowing for the use of a fluorophore with high quantum yield (15).

Fiber-optic based imaging has also become increasingly versatile in recent years as fiber components have decreased in size and gained functionality (16). Flexible fiber-optic endoscopy using optical probes that are typically a few millimeters in diameter have been used to imaging hollow tissue cavities such as the cervix or digestive tract (17, 18)

A fiber based microendoscope coupled into a whole-animal imaging system could allow for excitation light to be delivered inside an animal model. This would greatly enhance the intensity that could be achieved inside the animal, as the optical path length between the source and fluorophore could be decreased. In addition, such a system could allow for multi-scale imaging, where microscopic imaging could be obtained simultaneously with macroscopic whole-animal images.

2.2 Respiratory Disease

Respiratory diseases have a major impact on global health. It is necessary to consider disability and years of life lost as well as mortality to assess a conditions burden on health (19). Respiratory diseases rank at the top for burden, resulting in >8 million deaths per year. Thus, improved prevention and treatment is critical to improving human

health globally. Despite this, respiratory infections are not rapidly diagnosed, due to difficulty in identification of the agent. The development of imaging technology for respiratory agents is complicated by the small size of the infectious agents, usually <1 µm, and their ability to infect multiple organs, with the primary portal being the lungs. Despite this, the development of imaging for respiratory infections has the potential for tremendous impact on human health due to the number of individuals affected (20).

Of all respiratory infections, tuberculosis (TB) is the leading cause of death in the world by a bacterial infection, including the leading cause of death for HIV infect patients (21). Approximately 1.8 billion people are infected with TB, and an estimated 9 million new cases are reported annually. Around 2 million people die each year from TB worldwide (22). Several different technologies exist for detection of the disease, including a fiber-optic immune-sensor (23) and a transdermal skin patch (24). Additionally, TB has been studied using IVIS imaging systems (25), but these studies often rely on infection levels that are orders of magnitude greater than the infectious dose, making the study of physiologically relevant infections difficult.

Mycobacterium tuberculosis (MTB) is the bacterium responsible for tuberculosis infections. The disease is spread by droplet nuclei released during expectoration from a patient infected with pulmonary or laryngeal tuberculosis. The active disease is often characterized by a chronic cough, accompanied with bloody sputum. Additionally, patients often suffer from fever and weight loss. TB has an incubation period that can range from a few months to a few years following exposure, resulting in difficulty in diagnosis early during infection (26).

Bacillus Calmette-Guérin (BCG) is a vaccine against tuberculosis that is prepared from a strain of live, attenuated bovine tuberculosis (27). As a vaccine, BCG has shown widely varying efficacy depending on the group being vaccinated, with some people groups showing a 0% effect. Because of its similarity to TB, and its lack of virulence in humans, BCG is commonly used in TB related research (8, 28, 29). BCG was chosen for these experiments as a substitute for TB for these reasons. Additionally, work by Kong et al developed novel fluorescent tags that can be used to selectively identify TB (30). For these experiments, tdTomato was selected as the fluorophore to be expressed by BCG. tdTomato was chosen for several reasons, including its high quantum yield and brightness (the product of quantum yield and extinction coefficient). As a red-shifted protein, tdTomato also offers lower attenuation due to tissue absorption and scattering, allowing for more sensitive detection of its fluorescent emission.

3   OPTICAL SYSTEM DESIGN

As fiber based microendoscopes have previously been developed, the design of the optical system followed closely that of a system built for *ex vivo* imaging of bacterial infections (29). Slight modifications were made to this system to allow it to fit within the confines of the mouse lung, where the outer diameter of the fiber bundle is limited to roughly 600 µm. A detailed discussion of the microendoscope is provided in section 2.1, followed by a discussion of how the optical system was incorporated into a commercial whole-animal imager for multi-scale imaging.

3.1 Fiber Microendoscope Design

Figure 1 illustrates the fluorescence microendoscope that was constructed for bacterial detection. The basic design is similar to the system previously reported for use in bacterial imaging in situ (29). A light emitting diode (Thorlabs M530L2) centered at 530 nm with a 31 nm bandwidth was used for fluorescence excitation. This wavelength was selected for use with tdTomato. Light from the diode is collimated and then passed through an excitation filter (Semrock FF01-531/40). The beam was then reflected off a dichroic mirror (Semrock FF562-Di) and launched into a fiber bundle (Sumitomo) by a 10x objective lens. The 0.66 mm outer diameter fiber bundle consists of 10,000 individual fibers. A 3 µm core-to-core spacing limits the microendoscopes resolution, and the 450 µm active area determines the field of view (31). Excitation light is guided by the fiber
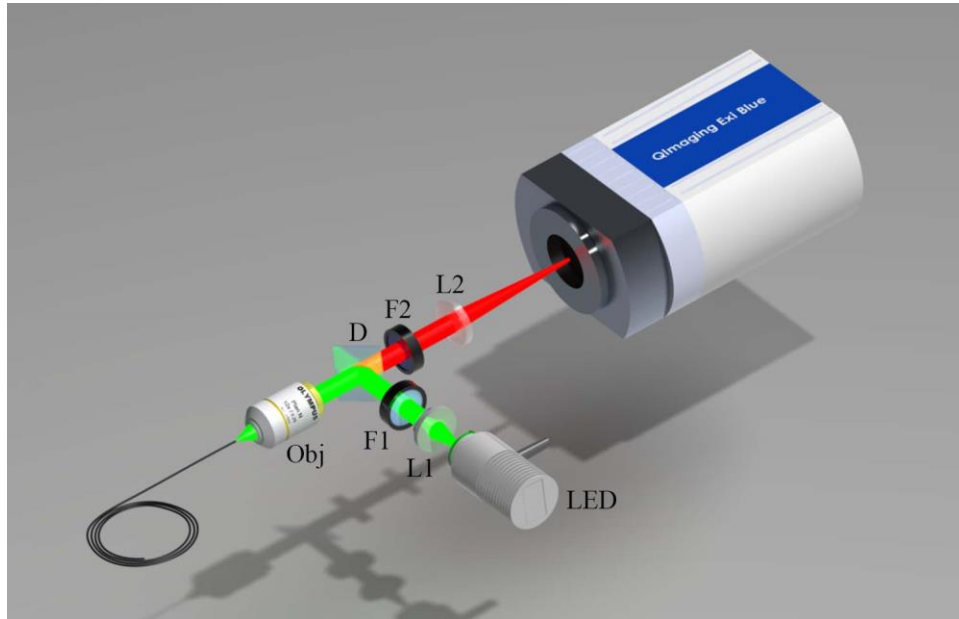
Figure 1: Illustration of the microendoscope system. LED: light emitting diode; L1: collimating lens; F1: excitation filter; D: dichroic beamsplitter; Obj: Microscope objective; F2: Emission filter; L2: focusing lens.

bundle to its distal tip, which can then be inserted into the lungs of an animal model. The typical output power from the fiber bundle was measured to be 350 µW. Insertion of the fiber into the mouse lungs was limited to the initial bifurcation of the lungs, as guiding the bundle beyond this point is difficult in the small space of a mouse lung, where fiber bend radii become a limit factor. Fluorescence emission from the bacterial infection is then collected by the same fiber bundle, filtered by a 572 nm longpass emission filter (Chroma HQ572LP), and then imaged onto a scientific grade 1.45 megapixel CCD camera (QImaging Exi Blue) with 6.45 µm x 6.45 µm pixel size.

9

3.2 Incorporation of Fiber Microendoscope Into Whole-Animal Imager

Multi-scale imaging of bacterial infections was achieved by integrating the microendscope into a whole animal imager (Perkin Elmer IVIS Lumina II). The fiber bundle was inserted into the whole animal enclosure through an access port located on the side of the system, shown in figure 2. To prevent any external light from entering the system, a 0.5 mm hole was drilled into a rubber stopper (VWR 59580-069) which was then inserted into the access port opening. The fiber bundle was then inserted through the hole in the rubber stopper, as shown in figure 2(b).
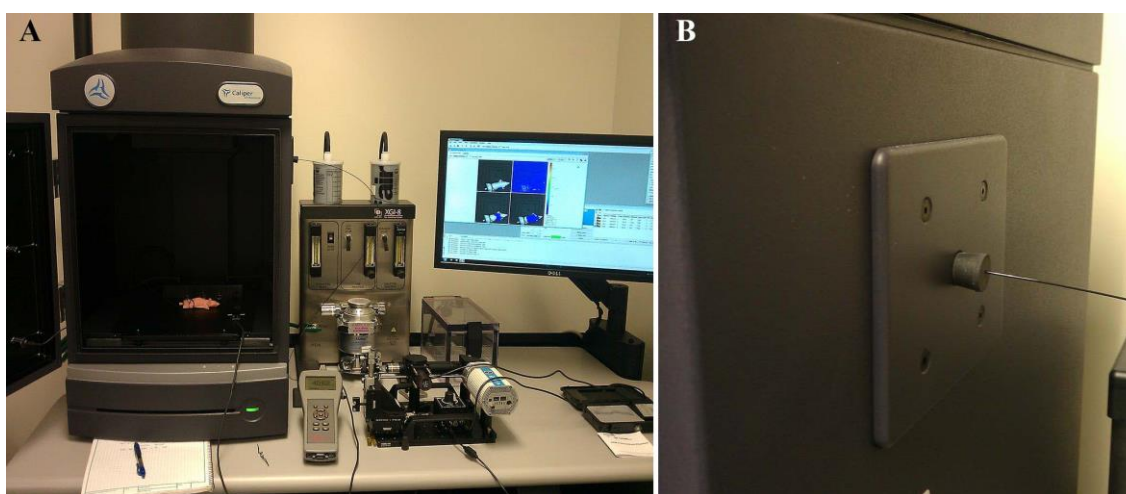
Figure 2: Integration of the fiber excitation source with the IVIS whole-animal imaging system. (A) shows both of the optical systems on the same bench top. (B)The fiber is coupled via a test tube stopper placed into the access port of the IVIS system.

The IVIS Lumina II imaging system operates in an epi-illuminations mode, where the excitation source and collection optics are both located above the animal stage. The excitation light is generated from a filtered lamp, and broadly dispersed over the entire sample stage to provide relatively even field illumination. Epi-illumination system

traditionally suffer from relatively poor depth sensitivity (2). The signal generated from epi-illumination systems decreases exponentially with depth, thus the images are surface-weighted. This is particularly the case when using fluorescent probes that excite with shorter wavelengths where hemoglobin absorption is stronger (15).

While providing the ability to acquire both macroscopic and microscopic images of bacterial infections from the same animal, the combination of the two optical systems also alleviates some of the individual limitations of each. First, the IVIS CCD can be used to localize and track the fiber bundle position inside the animal, allowing for proper positioning of the distal tip prior to data collection. More sophisticated whole-animal imaging systems that combine tomographic imaging capabilities could allow for even more accurate determination of the location of the fiber tip. In addition to this, the microendoscope source can serve as the excitation source for the whole-animal imager. By delivering the excitation light internally, the attenuation of the excitation radiation by tissue structures such as the chest wall is greatly decreased, allowing for an increase in the effective excitation intensity inside the region of interest. Figure 3(a) shows a mouse with its chest wall opened, where it can be seen that the excitation light scatters throughout the majority of the volume of the lungs, allowing for excitation of any fluorophore present in the lungs. Figure 3(b) depicts a typical microendoscope image obtained from the fiber bundle. Additionally, autofluorescence generated from a wide variety of molecules present in living tissue often can limit the detection sensitivity of whole animal imaging, especially when the desired signal is deeply embedded inside the animal (32, 33). By exciting directly at the location of interest, autofluorescence signal can be significantly reduced. This, in

combination with the increase in localized excitation intensity, allows for the potential detection of lower bacterial inocula.
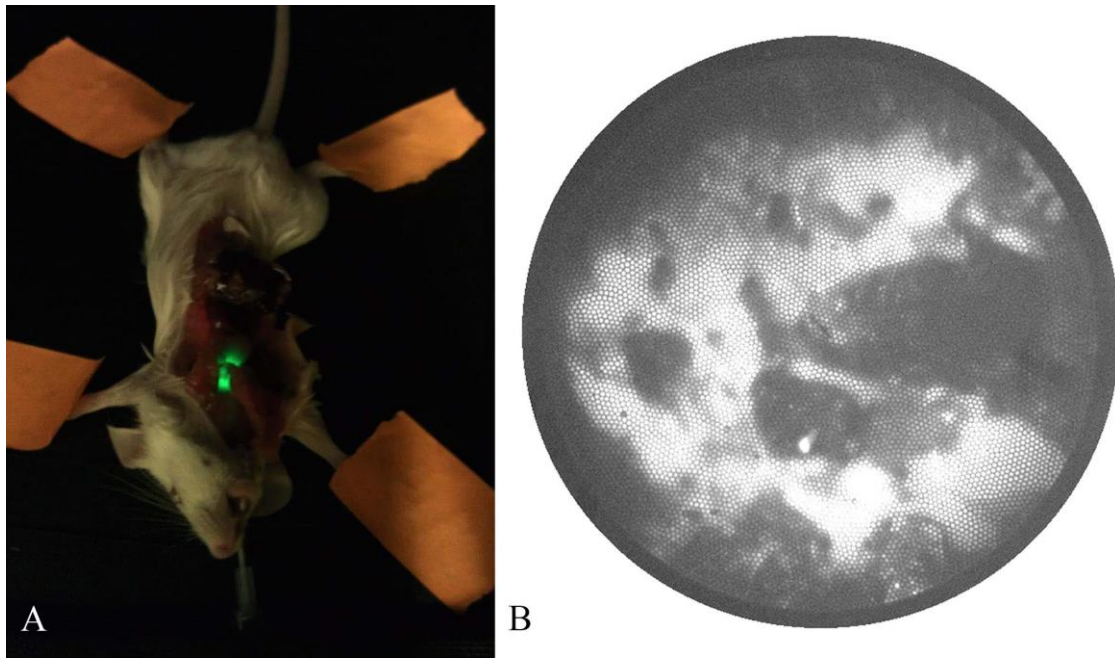
Figure 3: Images showing the coupling of the fiber microendosope into an animal placed inside an IVIS imaging system and a representative fluorescence microendoscope image. (A) Image of mouse with opened chest wall. This shows how despite the limitations on placement of the fiber bundle, and how excitation light illuminates the entire volume of the lungs due to scattering. (B) Representative fiber bundle image of bacterial infection.

Due to the lack of a collection lens on the distal tip of the fiber bundle, any images collected from this system *in vivo* where difficult to quantify with regards to bacterial signal. Signal could deviate greatly from animal to animal for those exposed to the same inoculation dose due to the location of the bacteria inside the lung. For this reason, these images served more as a guide when placing the fiber than as a quantitative means to assess the number of bacteria present inside the lung. The average intensity of these images can still be calculated to provide some feedback on the signal present, which could aid in positioning the fiber for optimal excitation for whole-animal imaging. To do this, a custom

MATLAB script was run on the collected image. The code for this can be found in appendix A.

4 IMAGE RESPIRATORY BACTERIAL INFECTIONS *IN VIVO* USING THE COMBINED MULTI-SCALE IMAGING SYSTEM

4.1 Imaging of Animal Model

To evaluate the enhancement in detection for whole-animal imaging using an internal excitation source, the detection of respiratory infections of *Mycobacterium bovis* Bacillus Calmette Guerin (BCG) was studied. BCG is an attenuated form of the live bovine tuberculosis bacillus, *Mycobacterium bovis* and used as a vaccine for *Mycobacterium tuberculosis*. BCG was chosen for this study for safety considerations, owing to its lack of virulence in humans. However, their ability to infect and persist within mammalian tissue is similar to the pathogenic mycobacteria (34). tdTomato was selected as the fluorescent protein for reasons described in (29) including its superior quantum yield as compared to the enhanced form of green fluorescent protein (35) and it being a red-shifted protein (15). In addition, previous work by Y. Kong et al. demonstrated superior detection limits with tdTomato labeled BCG as opposed to BCG expressing EGFP (13).

All animal studies were approved by the Texas A&M Institutional Animal Care and Use Committee. In this study, 18 female Balb/C mice were anesthetized and intratrachealy infected with tdTomto expressing BCG ranging from 10^1 to 10^5 CFU or a 10^5 CFU negative control. The procedure for infection was previously described in detail in (25). Three mice were infected for each inoculation group including three controls. The mice were then placed on the IVIS stage in a ventral position, and the paws were secured

to the stage. The fiber bundle was inserted into an intratracheal catheter until it was in proximity with the tracheal wall, and fluorescence signal could be observed using the microendoscope. The fiber bundle was marked to ensure the insertion distance was similar between animals, and to help guide the fiber insertion for the negative control animals. The fiber bundle was also secured to the stage to ensure it did not move when the stage height was adjusted during imaging.

Two imaging sequences were collected for each animal using the IVIS acquisition software. First, internal excitation of the bacterial infections was performed with the fiber bundle excitation source turned on, and the IVIS excitation set to "block." Fluorescence images were then collected with the filter wheel set to 580, 600, 620, and 640 nm, as well as the "open" setting which was used to localize the tip of the fiber bundle inside the animal. All images were acquired using the automatic exposure calculation performed by the Living Image software. Following this, the microendoscope excitation source was turned off, and the excitation filter for the IVIS system was set to 535 nm. Fluorescence emission was then recorded for the same range of emission filter settings. Following imaging, each animal was sacrificed, and the lungs were excised. The lung tissue was then homogenized, and the bacteria present quantified by colony viability counts following one month of bacterial culture.

4.2 IVIS Epi-Illumination Excitation

To provide a comparison between whole animal imaging using internal excitation and epi-illumination, images were acquired using the IVIS excitation and detection.

Representative images for infections of 10^4 and 10^5 CFU tdTomato labeled BCG are shown in figure 4(a-b) respectively. A representative image of the 10^5 CFU negative control is shown in figure 4(c).

All images were acquired using identical imaging parameters. The emission filter was varied from 580 nm to 640 nm for each sample. Each filter has an approximate bandwidth of 20 nm. Spectral unmixing was performed with the Living Image Software to attempt to separate background from the tdTomato fluorescence using the images from each emission filter. As can be seen from the images in figure 4, bacterial signal in the lungs was not detectable over tissue autofluorescence and fluorescence signal generated in the gastrointestinal track and bladder, even after post-processing.
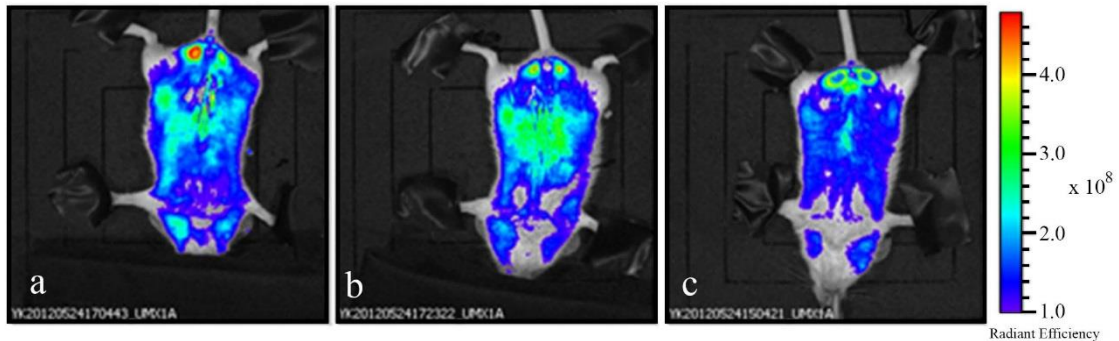
Figure 4: IVIS images of bacterial infection collected using the system's epi-illumination source for (A) 10^4, (B) 10^5 CFU tdTomato expressing BCG, and (C) 10^5 CFU BCG with vector backbone. Scale bar units are in (photons/sec/cm^2)/sr)/(μW/cm^2).

4.3 Whole-Animal Imaging Using Internal Fiber Excitation

Images acquired using the microendoscope as the excitation source are shown in figure 5. Representative images for 10^1, 10^2, 10^3, 10^4, and 10^5 CFU are shown in figure 5(a-e) respectively and an image of the 10^5 CFU negative control is shown in figure 5(f). Spectral unmixing was also performed using the same Living Image spectral unmixing

algorithm. Fluorescence images were then scaled such that no signal was left present for the negative control animals.
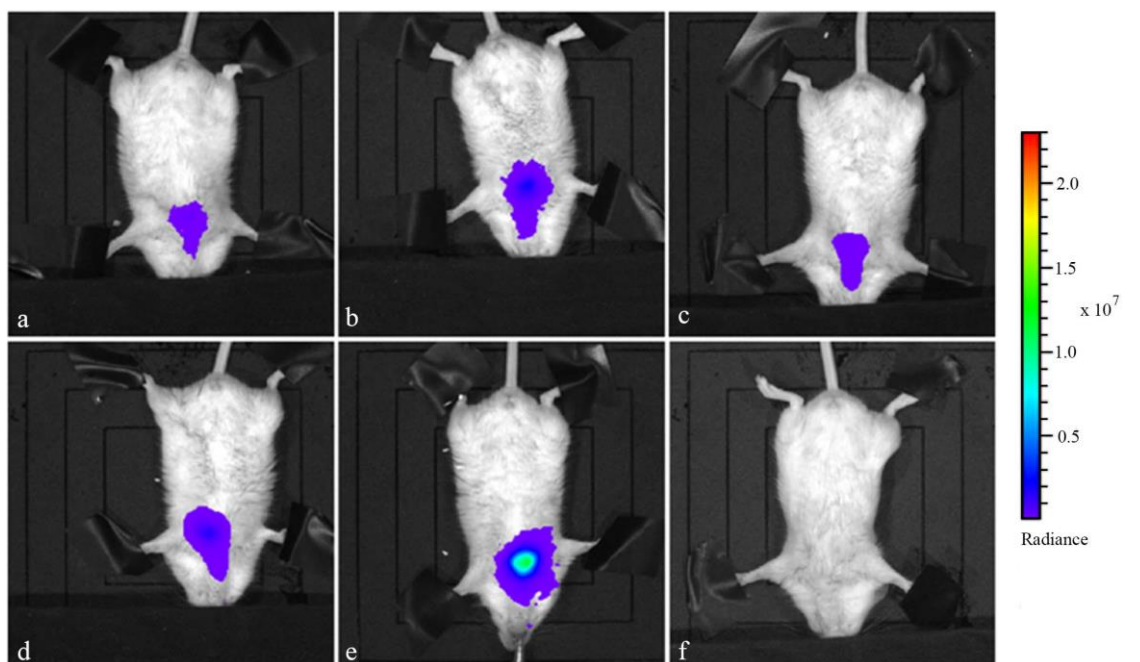
Figure 5: : IVIS images acquired using the internal fiber excitation source for (A) 10^1, (B) 10^2, (C) 10^3, (D) 10^4, (E) 10^5 CFU tdTomato expressing BCG and (F) 10^5 CFU BCG with vector backbone. The images were scaled such that no signal remained on the control.

4.4 Image Analysis

To assess the detection limits of the internal excitation scheme, average fluorescence intensities for each animal were calculated over the entire field of view following spectral unmixing. The signal measured for the three animals in each inoculation group was then averaged together, and plotted in figure 6. The error bars indicate one standard deviation

for each of these groups. An increasing trend is seen in the average fluorescence intensities with increasing infection levels with the exception of the 10^3 CFU inoculum. For this dose, significant variability was seen in the measured fluorescence intensities, resulting in a large standard deviation. A Student's t-test was used to determine statistically significant detection levels as compared to the negative control. P values for each group are displayed in figure 6 next to their corresponding data point. A value of $p <$ 0.05 was taken to indicate statistical significance. The lowest detectable inoculation using measured is 10^4 CFU (p-value = 0.047). The 10^3 CFU inoculums had the largest p-value (0.199), due to the large variation in measured intensity.

Images acquired with the IVIS excitation can be represented in calibrated units, allowing for easy comparison between multiple animals and for comparison of images
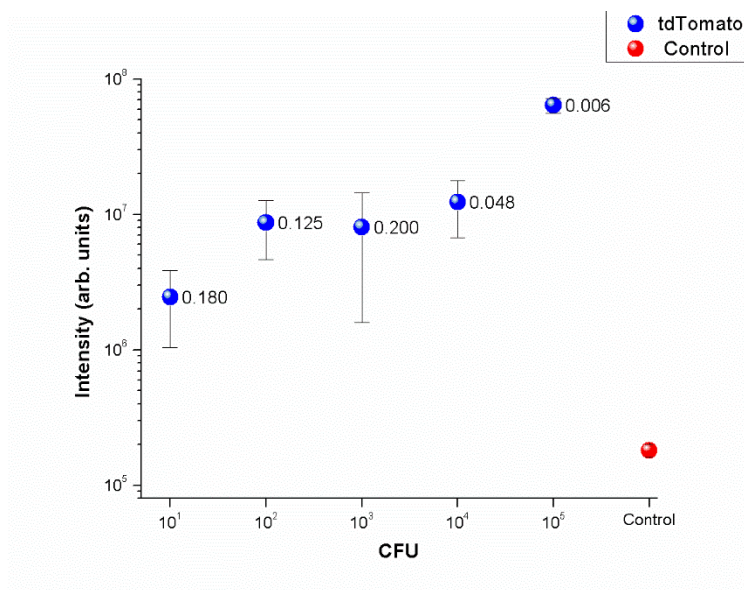
Figure 6: Quantification of the fluorescence signal for each inoculation dose. The error bars represent one standard deviation for each group. P-values for each group appear next to the data point, where $p < 0.05$ was deemed statistical

acquired at over time following infection. This calibration will not remain constant when using the fiber bundle as an excitation source. Additionally, signal detected will directly depend on the placement of the fiber inside the animal. Placement of the fiber into the stomach as opposed to the lungs will result in a significant decrease in the measured fluorescence. Images obtained with the fiber microendoscope proved to be useful for guidance to help avoid this. Due to variations in the location of the bacterial infection inside the lung, and the limitation of insertion beyond the initial bifurcation of the lungs, it is difficult to accurately quantify fluorescence signal measured with the microendoscope.

A detection limit of 10^4 CFU still presents a significant increase in detection sensitivity over the limits of epi-illumination whole-animal imaging. In addition, it is possible that with an increase in the number of mice, this detection limit could actually be lower than suggested by the current study. Trans-illumination systems, where the laser source and detector are located on opposite sides of the animal also provide enhanced detection sensitivities as compared to their epi-illumination counterparts. As excitation and emission must be transmitted through the entire animal, these systems inherently contain information from deep inside the tissue and are only weakly affected by the depth of the fluorophore, as opposed to the exponential dependence of the epi-illumination systems. Because of these things, trans-illumination systems are more ideally suited for detection of fluorescence from the respiratory system. Internal excitation has the potential to be more sensitive yet, but further comparisons are needed to evaluate this possibility.

5   SUMMARY AND CONCLUSIONS

We have demonstrated a novel method for whole-animal fluorescence imaging. By incorporating a microendoscope into a whole animal imaging system, the detection sensitivity of the combined system can be enhanced by at least 3 orders of magnitude. Bacterial infections were detected with statistical significance (p>0.05) at 10^4 CFU and greater. With IVIS excitation and detection, bacterial infections at 10^7 CFU could not be detected in vivo. An increase in the number of animals examined with this technique could prove to further lower the detection limits shown to have statistical significance.

While the fiber microendoscope used for these experiments employed a fiber bundle to deliver excitation light to the lungs, a simple large core, multimode fiber could be used in its place. This would allow for additional increases in excitation power that could be delivered. In addition, the system could be further miniaturized and designed to operate solely on battery power. This would allow for imaging inside other whole-animal imaging system that lack any form of access port like the one found on the IVIS Lumina II.

While the combined system does offer promise to increase the sensitivity for detection of respiratory infections, several steps remain before this technology can be transitions to the use in research labs who focus on pathology. First, more work is required to calibrate the use of an internal illumination source into the IVIS imaging software. The IVIS system is calibrated with itself, allowing for quantitative comparison of images collected over time to monitor disease progression. When changing the excitation source,

the system must be recalibrated to ensure accurate comparison of images over time. Without this, it would be more difficult to study disease progression or therapeutic efficacy over an extended period of time. Second, to allow for coupling of a fiber based excitation source into any whole-animal imager, the system must be made compact enough to fit on a sample stage. Power for the excitation source must also be considered, where the source could either draw power from internal batteries, or from the stage of the IVIS system itself. This would remove the need for the access port that was required for coupling of the microendoscope into the IVIS system used in this report.

Despite these things, the combined system shows great potential for enhancing research into a variety of diseases ranging from cancer progression to providing better understanding of the spread of bacterial infections. Additionally, enhanced detection sensitivity could allow for the study of diseases in more physiologically relevant concentrations, allowing researchers to more quickly develop novel therapies.

REFERENCES

1. R. Yuste, "Fluorescence microscopy today," *Nature Methods* 2(12), 902-904
    (2005)

2. F. Leblond, S. C. Davis, P. A. Valdés and B. W. Pogue, "Pre-clinical whole-body
    fluorescence imaging: Review of instruments, methods and applications," *Journal
    of Photochemistry and Photobiology B: Biology* 98(1), 77-94 (2010)

3. M. Baker, "Whole-animal imaging: The whole picture," *Nature* 463(7283), 977-
    980 (2010)

4. V. Ntziachristos, C.-H. Tung, C. Bremer and R. Weissleder, "Fluorescence
    molecular tomography resolves protease activity in vivo," *Nature Medicine* 8(7),
    757-761 (2002)

5. G. Tamgüney, K. P. Francis, K. Giles, A. Lemus, S. J. DeArmond and S. B.
    Prusiner, "Measuring prions by bioluminescence imaging," *Proceedings of the
    National Academy of Sciences* 106(35), 15002-15006 (2009)

6. J. Chen, C.-H. Tung, U. Mahmood, V. Ntziachristos, R. Gyurko, M. C. Fishman,
    P. L. Huang and R. Weissleder, "In vivo imaging of proteolytic activity in
    atherosclerosis," *Circulation* 105(23), 2766-2771 (2002)

7. D. E. Sosnovik, M. dudes and A. author, "Fluoorescence tomography and magnetic
    resonance imaging of myocardial macrophage infiltration in infarcted myocardium
    in vivo," *Circulation* 115(11), 1384-1391 (2007)

8. Y. Kong, H. Yao, H. Ren, S. Subbian, S. L. G. Cirillo, J. C. Sacchettini, J. Rao and
    J. D. Cirillo, "Imaging tuberculosis with endogenous β-lactamase reporter enzyme

fluorescence in live mice," *Proceedings of the National Academy of Sciences* 107(27), 12239-12244 (2010)

9.   J. M. Jabbour, M. A. Saldua, J. N. Bixler and K. C. Maitland, "Confocal endomicroscopy: instrumentation and medical applications," *Annals of Biomedical Engineering* 40(2), 378-397 (2012)

10.   A. Gmitro, "Confocal microscopy through a fiber-optic imaging bundle," *Optics Letters* 18(8), 565-567 (1993)

11.   J. Knittel, L. Schnieder, G. Buess, B. Messerschmidt and T. Possner, "Endoscope-compatible confocal microscope using a gradient index-lens system," *Optics Communications* 188(5), 267-273 (2001)

12.   P. M. Lane, S. Lam, A. McWilliams, J. C. Leriche, M. W. Anderson and C. E. Macaulay, "Confocal fluorescence microendoscopy of bronchial epithelium," *Journal of Biomedical Optics* 14(2), 024008 (2009)

13.   Y. Kong, S. Subbian, S. L. Cirillo and J. D. Cirillo, "Application of optical imaging to study of extrapulmonary spread by tuberculosis," *Tuberculosis* 89(S15-S17 (2009)

14.   J. N. Bixler, B. H. Hokr, M. L. Denton, G. D. Noojin, A. D. Shingledecker, H. T. Beier, R. J. Thomas, B. A. Rockwell and V. V. Yakovlev, "Assessment of tissue heating under tunable near-infrared radiation," *Journal of Biomedical Optics* 19(7), 070501-070501 (2014)

15.   N. C. Shaner, P. A. Steinbach and R. Y. Tsien, "A guide to choosing fluorescent proteins," *Nature Methods* 2(12), 905-909 (2005)

16. B. A. Flusberg, E. D. Cocker, W. Piyawattanametha, J. C. Jung, E. L. Cheung and M. J. Schnitzer, "Fiber-optic fluorescence imaging," *Nature Methods* 2(12), 941-950 (2005)

17. K. Carlson, M. Chidley, K. B. Sung, M. Descour, A. Gillenwater, M. Follen and R. Richards-Kortum, "In vivo fiber-optic confocal reflectance microscope with an injection-molded plastic miniature objective lens," *Applied Optics* 44(10), 1792-1797 (2005)

18. C. Liang, K.-B. Sung, R. R. Richards-Kortum and M. R. Descour, "Design of a high-numerical-aperture miniature microscope objective for an endoscopic fiber confocal reflectance microscope," *Applied Optics* 41(22), 4603-4610 (2002)

19. G. J. Wijnands, "Diagnosis and interventions in lower respiratory tract infections," *The American Journal of Medicine* 92(4), S91-S97 (1992)

20. M. B. Beasley, "The pathologist's approach to acute lung injury," *Archives of Pathology and Laboratory Medicine* 134(5), 719-727 (2010)

21. W. H. Organization, "Tuberculosis fact sheet. 2011," (2011).

22. Centers for Disease Control and Prevention (CDC). Reported tuberculosis in the United States, 2006. Atlanta, GA: US Department of Health and Human Services, CDC; 2007

23. M. Taniguchi, E. Akai, T. Koshida, K. Hibi, H. Kudo, K. Otsuka, H. Saito, K. Yano, H. Endo and K. Mitsubayashi, "A fiber optic immunosensor for rapid bacteria determination," in *3rd Kuala Lumpur International Conference on Biomedical Engineering 2006*, pp. 308-311, Springer (2007).

24. R. M. Nakamura, L. Einck, M. A. Velmonte, K. Kawajiri, C. F. Ang, C. E. Delasllagas and C. A. Nacy, "Detection of active tuberculosis by an MPB-64 transdermal patch: a field study," *Scandinavian Journal of Infectious Diseases* 33(6), 405-407 (2001)

25. Y. Kong, A. R. Akin, K. P. Francis, N. Zhang, T. L. Troy, H. Xie, J. Rao, S. L. Cirillo and J. D. Cirillo, "Whole-Body Imaging of Infection Using Fluorescence," *Current Protocols in Microbiology* 2C. 3.1-2C. 3.21 (2011)

26. K. Todar, *Todar's Online Textbook of Bacteriology*, University of Wisconsin-Madison Department of Bacteriology (2006).

27. G. A. Colditz, C. S. Berkey, F. Mosteller, T. F. Brewer, M. E. Wilson, E. Burdick and H. V. Fineberg, "The efficacy of bacillus Calmette-Guerin vaccination of newborns and infants in the prevention of tuberculosis: meta-analyses of the published literature," *Pediatrics* 96(1), 29-35 (1995)

28. C. Demangel, A. G. Bean, E. Martin, C. G. Feng, A. T. Kamath and W. J. Britton, "Protection against aerosol Mycobacterium tuberculosis infection using Mycobacterium bovis Bacillus Calmette Guérin-infected dendritic cells," *European Journal of Immunology* 29(6), 1972-1979 (1999)

29. N. Mufti, Y. Kong, J. D. Cirillo and K. C. Maitland, "Fiber optic microendoscopy for preclinical study of bacterial infection dynamics," *Biomedical Optics Express* 2(5), 1121 (2011)

30. Y. Kong and J. D. Cirillo, "Reporter enzyme fluorescence (REF) imaging and quantification of tuberculosis in live animals," *Virulence* 1(6), 558-562 (2010)

31. T. J. Muldoon, M. C. Pierce, D. L. Nida, M. D. Williams, A. Gillenwater and R. Richards-Kortum, "Subcellular-resolution molecular imaging within living tissue by fiber microendoscopy," *Optics Express* 15(25), 16413-16423 (2007)

32. A. W. K. N. Billinton, "Seeing the wood through the trees: a review of techniques for distinguishing green fluorescent protein from endogenous autofluorescence," *Anals of Biochemistry.* 291(175-197 (2001)

33. G. A. Wagnieres, W. M. Star and B. C. Wilson, "In Vivo Fluorescence Spectroscopy and Imaging for Oncological Applications," *Photochemistry and Photobiology* 68(5), 603-632 (1998)

34. S. Gordon, M. Keshav and Stein, "BCG-Induced Granuloma Formation in Murine Tissues," *Immunobiology* 191(4), 369-377 (1994)

35. M. Goldgeier, C. A. Fox, J. M. Zavislan, D. Harris and S. Gonzalez, "Noninvasive imaging, treatment, and microscopic confirmation of clearance of basal cell carcinoma," *Dermatologic Surgery* 29(3), 205-210 (2003)

APPENDIX A: MATLAB CODE FOR IMAGE PROCESSING

The following MATLAB code was used to process the fiber microendoscope images acquired:

```matlab
clear all; close all;
Image = imread('image.tif','tif'); % script not automated, replace
'image' with file name of image to be processed.
img = double(Image);
background = 0; numB = 0; % for use in background removal
sum =0;
c =0;
A = zeros(1040,1392);
%Background removal
for i=1:150
    for j = 1:150
        background = background + img(i,j);
        numB = numB + 1;
    end
end
AvgBackground = background./numB;
newImg = img - AvgBackground;
figure(1);imagesc(newImg);colormap(gray);

for i=1:1047
    for j=1:1392
        if sqrt((i-515)^2+(j-730)^2)<=508    % Center, (x,y) = (730,515)
Radius = 508
            A(i,j) = 1;
            sum = sum + newImg(i,j);
            c=c+1;
        end
    end
end
figure;imagesc(Image);
figure;imagesc(Image);colormap(gray);
confirm = A.*newImg;
figure; imagesc(confirm);colormap(gray);
AvgIntensity = sum/c
```